Mesostructures

DOI: 10.1002/anie.200703627

Mesostructured Prussian Blue Analogues**

*Xavier Roy, Laurence K. Thompson, Neil Coombs, and Mark J. MacLachlan**

Mesoporous silica, a form of SiO_2 with periodic organization of channels on the nanometer length scale, is formed by an aqueous liquid-crystal-templating route.[1] This approach has been used to prepare a wide range of oxides[2] and heavier chalcogenides,[3] but making mesostructured materials with other compositions remains a significant challenge.[4] Liquid-crystal-templated materials composed of metal–organic coordination networks are particularly attractive targets since crystalline microporous coordination frameworks are promising candidates for asymmetric catalysis and separations,[5] and storage of small molecules (e.g., H_2 and CH_4).[6] Herein we report a strategy to synthesize mesostructured coordination frameworks based on Prussian blue (PB) analogues. We illustrate the diversity of these new materials with representative monometallic and bimetallic materials that form lamellar, hexagonal, and cubic phases. The materials formed from octahedral Fe^{III}/Fe^{II} coordination environments are the first examples of liquid-crystal-templated mesostructured solids to exhibit valence delocalization and magnetic interactions.

We selected Prussian blue as the prototype for metal–organic mesostructures. PB, the first synthetic coordination compound, was prepared accidentally by Diesbach and Dippel in 1704 and has endured a rich history.[7] Owing to its intense blue color, PB has long been used as a dye and in paints used by artists including Picasso, Monet, and van Gogh. The archetypical PB is a cubic network of $[Fe_4\{Fe(CN)_6\}_3]\cdot(H_2O)_n$ in which the Fe atoms lie at the lattice points and the cyanide groups are bridging, and the family now includes diverse cyanometallates with similar formulae. Recently, the use of these generic PB analogues as coatings,[8] photomagnetic switches,[9] electrocatalysts,[10] and sensors[11] has been explored. Even though bulk crystallites of PB may be adequate for these applications, the invention of nanostructured PB may provide materials with high surface area, porosity, and anisotropic magnetic behavior, properties that may be desirable for other applications. Prussian blue nanocrystals,[12] nanowires,[13] and Langmuir monolayers[14] have been reported, but to date no examples of mesostructured PB are known.

We first attempted to prepare mesostructured PB by the condensation of $(C_{16}H_{33}NMe_3)_n[Fe(CN)_6]$ ($n=3$ or 4) with $FeCl_3$. Powder X-ray diffraction (PXRD) of the product showed only broad peaks assigned to microcrystalline PB and no evidence for a mesostructure. Infrared (IR) spectroscopy confirmed that the surfactant was excluded from the product.

Recognizing that it would be difficult to circumvent crystallization of the thermodynamically stable PB lattice, we prepared a family of alkyl pyrazinium surfactants (**1**) that could tether to the PB precursors to enable the isolation of a kinetically controlled mesostructure. Addition of **1** in hot water to an aqueous solution of $Na_3[Fe(CN)_5NH_3]\cdot 3H_2O$ caused rapid precipitation of **2**. Deep blue compound **2** has a coordination complex as its large polar head group bearing a charge of −2 and derives its color from a metal-to-ligand charge-transfer (MLCT) band. We anticipated that amphiphilic **2** would behave as a surfactant in water or formamide. Unfortunately, once isolated, complex **2** proved to be impossible to redissolve in formamide without partial decom-

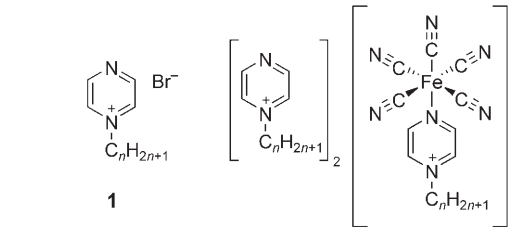

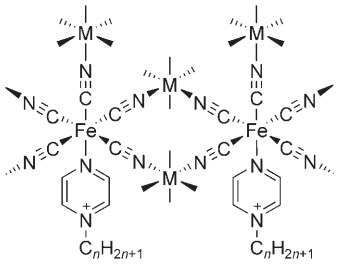

$M^xFe^{II}C_n$

(x=I, II, III)

[*] X. Roy, Prof. M. J. MacLachlan
Department of Chemistry
University of British Columbia
2036 Main Mall, Vancouver, BC, V6T 1Z1 (Canada)
Fax: (+1) 604-822-2847
E-mail: mmaclach@chem.ubc.ca
Prof. L. K. Thompson
Department of Chemistry
Memorial University of Newfoundland
St. John's, NL, A1B 3X7 (Canada)
Dr. N. Coombs
Centre for Nanostructure Imaging
Department of Chemistry
University of Toronto
80 St. George Street, Toronto, ON, M5S 3H6 (Canada)

[**] We thank the Natural Sciences and Engineering Research Council of Canada and UBC for funding. X.R. thanks the FQRNT and NSERC for postgraduate scholarships. We thank Dev Sharma and Danny Leznoff (Simon Fraser University) for obtaining the Mössbauer data, Robert Thompson (UBC) for helpful discussions, and Erin MacLachlan for assistance with the text.

Supporting information for this article is available on the WWW under http://www.angewandte.org or from the author.

position. Instead, we used **2** in situ in a one-pot synthesis of coordination mesostructures. First, $Na_3[Fe(CN)_5NH_3]\cdot 3H_2O$ was slowly added to a solution of **1** in hot formamide to give a blue solution characteristic of amphiphilic iron complex **2**. Next, a transition-metal salt (e.g., $Fe(NO_3)_3$, $Cu(NO_3)_2$, CuCl, $Mn(O_2CCH_3)_2$, $Ni(NO_3)_2$, $Zn(NO_3)_2$, $Gd(NO_3)_3$, or $Er(NO_3)_3$) in formamide was added to precipitate a richly colored solid. Water can also be used as a solvent, but formamide yields better ordered materials. We label our materials with the general formula $M^xFe^{II}C_n$, whereby M represents the linking metal with oxidation state x, Fe^{II} designates the cyanometallate headgroup, and C_n specifies the number of carbon atoms in the alkyl chain (C_nH_{2n+1}) of the tethered alkyl pyrazinium. For example, a material prepared using octadecylpyrazinium bromide (**1**, $n = 18$), $Na_3[Fe(CN)_5NH_3]\cdot 3H_2O$, and $Zn(NO_3)_2$ as linking agent is referred as $Zn^{II}Fe^{II}C_{18}$.

Figure 1 A shows the PXRD patterns for microcrystalline PB and two representative materials $Fe^{III}Fe^{II}C_{22}$ and $Er^{III}Fe^{II}C_{18}$. Low-angle peaks ($2\theta < 5°$) for $Fe^{III}Fe^{II}C_{22}$ and $Er^{III}Fe^{II}C_{18}$ that correspond to neither **1** nor **2** confirm the existence of a mesostructured product. The higher-angle peaks are in the same region as those for bulk PB and suggest some order in the cyanometallate wall structure. PXRD patterns indicative of mesostructures were observed for all metal combinations used. In addition, a given metal combination reproducibly yields a given mesostructure (i.e., phase and order from PXRD) with the structural variability presumably arising from the different coordination numbers and geometries of the linking metals. Figure 1 B shows the low-angle regions of the PXRD patterns of four representative samples. $Er^{III}Fe^{II}C_{12}$ and $Fe^{III}Fe^{II}C_{20}$ both exhibit an intense low-angle peak at 37 and 40 Å, respectively, and a weak unresolved feature at $2\theta \approx 4$–$5°$, which, according to the transmission electron microscopy (TEM), can be assigned to the overlapping (11) and (20) reflections of a hexagonal *p6mm* symmetry mesostructure. Interestingly, when Cu^I is used as linking metal, a material is obtained that has a diffraction pattern with five diffraction peaks that index to a cubic phase. Disorder present in the structure, however, prevented us from obtaining satisfactory TEM images of this product. Figure 1 B, trace d, shows the lamellar order for the Er^{III}/Fe^{II} system, prepared using the C_{22} alkyl chain. The chain length used in these preparations affects the dimensions of the mesostructures and the extent of order in the materials, as illustrated for $Fe^{III}Fe^{II}C_n$ (Figure 1 C). Upon extending the chain length from 12 to 22 carbon atoms, the first diffraction peak shifts to lower angle and all low-angle peaks increase in intensity, which is characteristic of improved order.

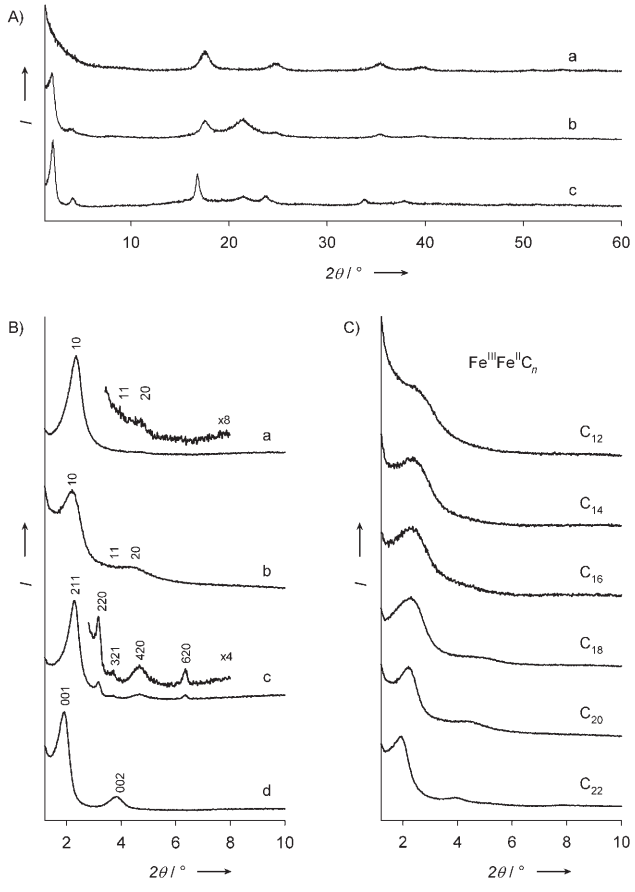

Figure 1. A) Wide-angle PXRD patterns of microcrystalline PB (a), $Fe^{III}Fe^{II}C_{22}$ (b), and $Er^{III}Fe^{II}C_{18}$ (c). B) Low-angle PXRD patterns of 2D hexagonal $Er^{III}Fe^{II}C_{12}$ (a), 2D hexagonal $Fe^{III}Fe^{II}C_{20}$ (b), cubic $Cu^IFe^{II}C_{18}$ (c), and lamellar $Er^{III}Fe^{II}C_{22}$ (d). C) PXRD patterns showing the evolution of the $Fe^{III}Fe^{II}C_n$ mesostructure as the alkyl chain length is increased from 12 to 22 carbon atoms.

Figure 2 shows representative TEM images of the mesostructured PB materials. We recorded micrographs both perpendicular and parallel to the channels for $Er^{III}Fe^{II}C_{12}$ (Figure 2 A,B). Both images show a hexagonally packed structure of cylindrical channels with an average diameter of 30–35 Å. Figure 2 C confirms the 2D hexagonal structure for $Fe^{III}Fe^{II}C_{20}$, and Figure 2 D shows the lamellar structure of $Er^{III}Fe^{II}C_{22}$, which has an interplane distance of approximately 40 Å (compared with ca. 46 Å by PXRD).

The composition and connectivity of the structures were established by elemental analysis (EA), energy-dispersive X-ray (EDX) analysis, thermogravimetric analysis (TGA), IR spectroscopy, and UV/Vis spectroscopy. EA of the materials

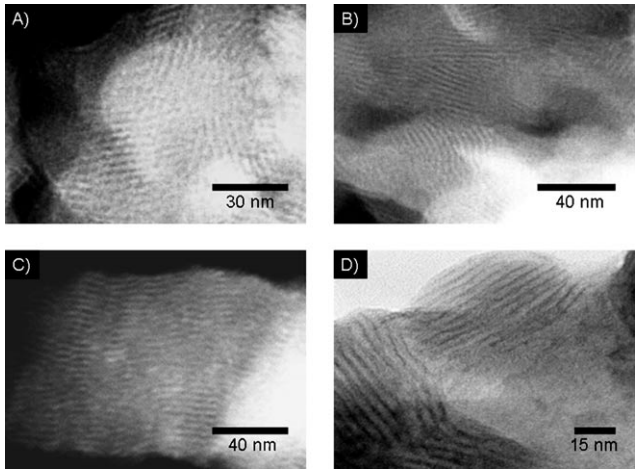

Figure 2. TEM images of A) $Er^{III}Fe^{II}C_{12}$ perpendicular to the channels; B) $Er^{III}Fe^{II}C_{12}$ parallel to the channels; C) 2D hexagonal $Fe^{III}Fe^{II}C_{20}$; D) lamellar $Er^{III}Fe^{II}C_{22}$. Images (A–C) were obtained in high-angle annular dark field (HAADF) mode and (D) was taken in bright field mode.

(Table S1 in the Supporting Information) confirms the incorporation of 5–25 wt % iron and the second metal in the structure. As expected, lengthening the alkyl chain generally increases the carbon content and decreases the fraction of metal and nitrogen. Atomic metal ratios (M^x/Fe^{II}) ranging from 0.7 to 3 are typically measured. EDX also showed low levels of halides and alkali metals in the samples; the remainder of the mass balance is likely oxygen from included or coordinated solvent, water, and counterions (e.g., NO_3^-). TGA of the materials showed 5–8 % weight loss below 200 °C, mainly attributed to the release of the solvent molecules or water trapped in the mesostructure. The main weight loss resulting from the decomposition of the alkyl pyrazinium ligand combined with the breakdown of the PB network occurs between 200 and 500 °C.

IR spectra of the mesostructured materials show peaks attributable to the alkyl pyrazinium moiety and to the pentacyanoferrate(II) unit. IR spectroscopy also confirmed that the walls of the mesostructures contain metal centers linked by bridging cyanide ligands. The three ν_{CN} stretching modes of the approximately C_{4v}-symmetrical $[Fe(CN)_5NH_3]^{3-}$ unit are in the range 2000–2150 cm^{-1}, with the strongest band at 2047 cm^{-1}. Replacing the ammine ligand with the π-accepting alkyl pyrazinium results in increased ν_{CN} stretching frequencies;[15] the most intense band is observed at 2069 cm^{-1} for unlinked **2**. Upon formation of the mesostructured material, the product shows a significantly broader ν_{CN} stretching band, which is always at higher frequency (2075–2105 cm^{-1}). It is well established that ν_{CN} modes for bridging cyanides appear at higher frequency than for terminal cyanides.[16]

Further evidence for the connectivity in the structures emerged from stability studies. The insoluble mesostructured materials retain their order (PXRD) after washing with formamide, hot water, hot alcohols, chlorinated solvents, and DMSO, or sonication in methanol and drying under vacuum for extended periods. For metal analysis, it was necessary to degrade samples in boiling H_2SO_4/HNO_3.

The intense color of PB arises from an intervalence charge-transfer (IVCT) band at around 720 nm (full width at half maximum (FWHM) = 410 nm). Our mesostructured materials have brilliant colors akin to PB, and their colors are dependent on the metal combination utilized. UV/Vis spectroscopy (Figure 3 A) verified valence delocalization in the mesostructured materials. The UV/Vis spectrum of unlinked **2** shows high-energy bands in the UV region as well as a broad MLCT absorption band[17] centered at 681 nm (FWHM = 210 nm). $Zn^{II}Fe^{II}C_{18}$, which is not expected to exhibit any valence delocalization since Zn^{II} has a d^{10} electronic configuration, displays a slightly blue-shifted, but otherwise unchanged MLCT band centered at 616 nm (FWHM = 224 nm). In contrast, mesostructured $Fe^{III}Fe^{II}C_{18}$ shows a significantly broader absorption band (FWHM = 486 nm) centered at 690 nm resulting from the overlap of the MLCT and the IVCT bands. All of the $Fe^{III}Fe^{II}C_n$ materials exhibit this broad IVCT band, which is characteristic of Robin and Day class II delocalization[18] between the cyanide-bridged metal centers. None of the mixed-metal mesostructures shows evidence of valence delocalization.

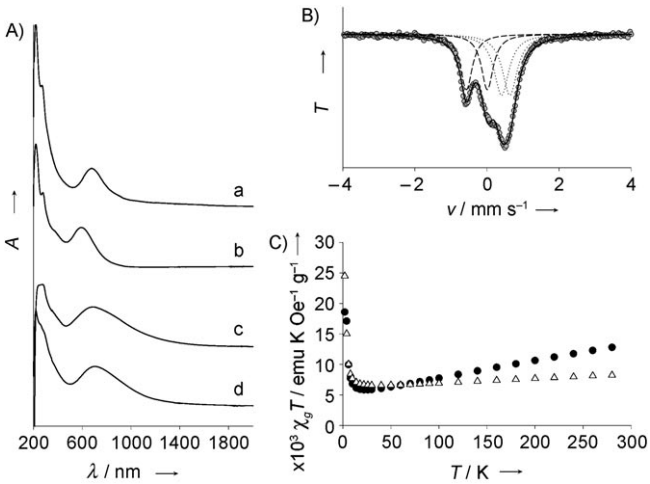

Figure 3. A) UV/Vis absorption spectra for unlinked **2** ($n = 18$) (a), $Zn^{II}Fe^{II}C_{18}$ (b), $Fe^{III}Fe^{II}C_{18}$ (c), and bulk PB (d). B) Mössbauer spectrum for $Fe^{III}Fe^{II}C_{18}$ at 300 K fitted as arising from two quadrupole doublets (● = data; solid line = fit). Site 1 (dotted lines) is assigned to high-spin Fe^{III}: isomer shift $\delta = 0.57$ mm s^{-1}, $\Delta E_Q = 0.23$ mm s^{-1}, area = 58 %; and site 2 (dashed lines) is assigned to low-spin Fe^{II}: $\delta = -0.28$ mm s^{-1}, $\Delta E_Q = 0.58$ mm s^{-1}, area = 42 %. C) Plots of $\chi_g T$ vs T at 0.1 T for $Fe^{III}Fe^{II}C_{18}$ (●) and for $Fe^{III}Fe^{II}C_{22}$ (△). Because the exact molecular structures are not known, the magnetic susceptibilities are calculated per gram of material (χ_g). Complex **2** is diamagnetic.

The room-temperature ^{57}Fe Mössbauer spectrum for $Fe^{III}Fe^{II}C_{18}$ (Figure 3 B) shows two quadrupole doublets assigned to high-spin Fe^{III} and low-spin Fe^{II}. The large quadrupole splitting (ΔE_Q) for Fe^{II} indicates significant distortion from octahedral geometry, as expected for an intact complex **2**.[19] The quadrupole splitting for Fe^{III} arises from its unsymmetrical coordination sphere composed of N-bonded cyanides and solvent molecules.

The magnetic properties of the mesostructured materials were investigated by using superconducting quantum interference device (SQUID) magnetometry. In PB, the Fe^{III} spin centers, which are separated by low-spin Fe^{II} centers, couple ferromagnetically at low temperature ($T_C = 5.6$ K).[20] Magnetometry measurements of $Fe^{III}Fe^{II}C_{18}$ and $Fe^{III}Fe^{II}C_{22}$ (Figure 3 C) show ferromagnetic interactions below 10 K, thus indicating that the magnetic order is preserved in the mesostructured PB analogues despite defects and wall curvature. $Ni^{II}Fe^{II}C_{18}$ and $Cu^{II}Fe^{II}C_{18}$ did not show spin interaction at low temperatures.

On the basis of our results, reaction of **1** and $Na_3[Fe(CN)_5NH_3]\cdot 3H_2O$ in formamide gives an amphiphilic intermediate that templates the formation of a mesostructured material upon addition of a second metal salt. PXRD and TEM show that the materials exhibit long-range periodic order on the nanometer scale, and can exhibit lamellar, hexagonal, or cubic phases. IR and UV/Vis spectra indicate that, analogous to PB, the metal centers of the mesostructured materials are connected by cyanide bridges. Figure 4 illustrates the idealized supramolecular assembly and resulting mesostructure. Although a ligand-assisted templating approach has been used for synthesizing metal-oxide frameworks,[21] the extension to metal cyanides is a new develop-

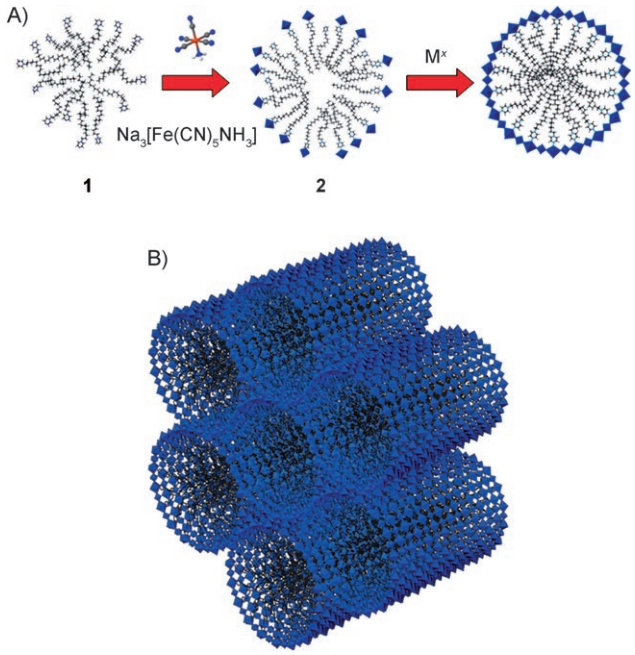

Figure 4. A) Synthetic approach and B) idealized structure of a hexagonal mesostructured PB analogue.

ment that will open the way to a variety of new mesostructured materials.

In summary, we report the first examples of mesostructured PB analogues. This new structurally diverse family of compounds can be synthesized with different combinations of transition metals and alkyl chain lengths. As these are the first examples of metal–organic liquid-crystal-templated mesostructures, we have demonstrated that liquid-crystal templating can be extended to coordination compounds to provide new materials with order on the nanometer scale. The PB analogues are also the first liquid-crystal-templated mesostructures to display valence delocalization and magnetic interactions in the framework. Furthermore, as the pentacyanoferrate(II) building block is part of the much larger cyanometallate family, we expect that this route to PB analogues will provide an array of mesostructures with tunable magnetic, optical, and electronic properties.

Experimental Section

Representative synthesis for $M^xFe^{II}C_n$ ($Fe^{III}Fe^{II}C_{18}$): $Na_3[Fe(CN)_5NH_3]\cdot 3H_2O$ (1.25 g) dissolved in formamide (25 mL) was added dropwise to a stirred solution of octadecylpyrazinium bromide (14.8 g) in formamide (150 mL) at 80 °C. The solution immediately turned dark blue. The solution was stirred for 10 min and then $Fe(NO_3)_3$ (12.4 g) in hot formamide (25 mL, 80 °C) was added dropwise. The mixture was stirred at 80 °C for 10 min and then allowed to sit at room temperature for 12 h. The precipitate was collected on a Büchner funnel and washed with formamide (80 °C), boiling ethanol, and water (80 °C), then dried under vacuum (yield: 3.1 g of blue powder). Similar procedures were used for the other materials, but varying the alkyl pyrazinium bromide and the linking metal salt.

Received: August 9, 2007
Published online: November 7, 2007

Keywords: magnetic properties · mesostructured materials · mixed-valent compounds · Prussian blue · supramolecular chemistry

[1] a) C. T. Kresge, M. E. Leonowicz, W. J. Roth, J. C. Vartuli, J. S. Beck, *Nature* **1992**, *359*, 710–712; b) J. S. Beck et al., *J. Am. Chem. Soc.* **1992**, *114*, 10834–10843.
[2] a) D. Zhao, J. Feng, Q. Huo, N. Melosh, G. H. Fredrickson, B. F. Chmelka, G. D. Stucky, *Science* **1998**, *279*, 548–552; b) M. Vettraino, M. L. Trudeau, D. M. Antonelli, *Adv. Mater.* **2000**, *12*, 337–341; c) U. Ciesla, S. Schacht, G. D. Stucky, K. K. Unger, F. Schüth, *Angew. Chem.* **1996**, *108*, 597–600; *Angew. Chem. Int. Ed. Engl.* **1996**, *35*, 541–543; d) B. J. Melde, B. T. Holland, C. F. Blanford, A. Stein, *Chem. Mater.* **1999**, *11*, 3302–3308; e) S. Inagaki, S. Guan, T. Ohsuna, O. Terasaki, *Nature* **2002**, *416*, 304–307; f) T. Asefa, M. J. MacLachlan, N. Coombs, G. A. Ozin, *Nature* **1999**, *402*, 867–871; g) A. Sayari, P. Liu, M. Kruk, M. Jaroniec, *Chem. Mater.* **1997**, *9*, 2499–2506; h) P. T. Tanev, T. J. Pinnavaia, *Science* **1995**, *267*, 865–867.
[3] a) M. J. MacLachlan, N. Coombs, G. A. Ozin, *Nature* **1999**, *397*, 681–684; b) P. V. Braun, P. Osenar, S. I. Stupp, *Nature* **1996**, *380*, 325–328; c) P. N. Trikalitis, K. K. Rangan, T. Bakas, M. G. Kanatzidis, *Nature* **2001**, *410*, 671–675.
[4] a) M. G. Kanatzidis, *Adv. Mater.* **2007**, *19*, 1165–1181; b) F. Schüth, *Chem. Mater.* **2001**, *13*, 3184–3195; c) G. S. Attard, P. N. Bartlett, N. R. B. Coleman, J. M. Elliott, J. R. Owen, J. H. Wang, *Science* **1997**, *278*, 838–840; d) G. S. Armatas, M. G. Kanatzidis, *Nature* **2006**, *441*, 1122–1125; e) D. Sun, A. E. Riley, A. J. Cadby, E. K. Richman, S. D. Korlann, S. H. Tolbert, *Nature* **2006**, *441*, 1126–1130.
[5] J. S. Seo, D. Whang, H. Lee, S. I. Jun, J. Oh, Y. J. Jeon, K. Kim, *Nature* **2000**, *404*, 982–986.
[6] H. Li, M. Eddaoudi, M. O'Keeffe, O. M. Yaghi, *Nature* **1999**, *402*, 276–279.
[7] K. R. Dunbar, R. A. Heintz, *Prog. Inorg. Chem.* **1997**, *45*, 283–391.
[8] A. A. Karyakin, *Electroanalysis* **2001**, *13*, 813–819.
[9] O. Sato, T. Iyoda, A. Fujishima, K. Hashimoto, *Science* **1996**, *272*, 704–705.
[10] S.-M. Chen, *J. Electroanal. Chem.* **2002**, *521*, 29–52.
[11] L. G. Beauvais, M. P. Shores, J. R. Long, *J. Am. Chem. Soc.* **2000**, *122*, 2763–2772.
[12] S. Vaucher, M. Li, S. Mann, *Angew. Chem.* **2000**, *112*, 1863–1866; *Angew. Chem. Int. Ed.* **2000**, *39*, 1793–1796.
[13] P. Zhou, D. Xue, H. Luo, X. Chen, *Nano Lett.* **2002**, *2*, 845–847.
[14] J. T. Culp, J.-H. Park, D. Stratakis, M. W. Meisel, D. R. Talham, *J. Am. Chem. Soc.* **2002**, *124*, 10083–10090.
[15] E. Waldhör, W. Kaim, J. A. Olabe, L. D. Slep, J. Fiedler, *Inorg. Chem.* **1997**, *36*, 2969–2974.
[16] S. F. A. Kettle, E. Diana, E. Boccaleri, P. L. Stanghellini, *Inorg. Chem.* **2007**, *46*, 2409–2416.
[17] H. E. Toma, J. M. Malin, *Inorg. Chem.* **1973**, *12*, 1039–1045.
[18] M. B. Robin, P. Day, *Adv. Inorg. Chem. Radiochem.* **1967**, *10*, 247–422.
[19] C. R. Johnson, R. E. Shepherd, *Inorg. Chem.* **1983**, *22*, 3506–3513.
[20] A. Ito, M. Suenaga, K. Ôno, *J. Chem. Phys.* **1968**, *48*, 3597–3599.
[21] D. M. Antonelli, J. Y. Ying, *Angew. Chem.* **1996**, *108*, 461–464; *Angew. Chem. Int. Ed. Engl.* **1996**, *35*, 426–430.

